THE JOURNAL OF PHYSICAL CHEMISTRY Letters

Letter

pubs.acs.org/JPCL

Biexciton Resonances Reveal Exciton Localization in Stacked Perovskite Quantum Wells

Madeline H. Elkins,[†] Ryan Pensack,[†] Andrew H. Proppe,[‡,§] Oleksandr Voznyy,[‡] Li Na Quan,[‡] Shana O. Kelley,[§] Edward H. Sargent,[‡] and Gregory D. Scholes*[,†]

[†]Department of Chemistry, Princeton University, Princeton, New Jersey 08544 United States

[‡]Department of Electrical and Computer Engineering, University of Toronto, Toronto, Ontario M5S 3G4, Canada

[§]Department of Chemistry, University of Toronto, Toronto, Ontario M5S 3G4, Canada

Supporting Information

ABSTRACT: Quasi-two-dimensional lead halide perovskites, $MA_{n-1}Pb_nX_{3n+1}$, are quantum confined materials with an ever-developing range of optoelectronic device applications. Like other semiconductors, the correlated motion of electrons and holes dominates the material's response to optical excitation influencing its electrical and optical properties such as charge formation and mobility. However, the effects of many-particle correlation have been relatively unexplored in perovskite because of the difficultly of probing these states directly. Here, we use double quantum coherence spectroscopy to explore the formation and localization of multiexciton states in these materials. Between the most confined domains, we demonstrate the presence of an interwell, two-exciton excited state. This demonstrates that the four-body Coulomb interaction electronically couples neighboring wells despite weak electron/hole hybridization in these materials. Additionally, in contrast with inorganic semiconductor quantum wells, we demonstrate a rapid decrease in the dephasing time as wells become thicker, indicating that exciton delocalization is not limited by structural inhomogeneity in low-dimensional perovskite.

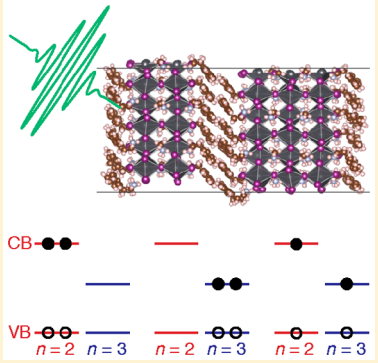

Quasi-two-dimensional (quasi-2D) lead halide perovskites, quantum confined materials consisting of few lead halide monolayers separated by an organic barrier layer, have seen remarkable growth in device applications[1] in recent years as more stable alternatives to three-dimensional perovskites with functional light emission[2] and photovoltaic efficiency.[3] Despite similarities in device efficiency, the basic photophysics of quasi-2D devices is greatly influenced by confinement, which is not present in the bulk. Despite early comparisons to quantum wells,[4] prior photophysical studies of these devices have ignored, with few exceptions,[5,6] the role of many-body interactions (the correlated motion of more than one exciton or carrier), which dominate the nonlinear response of quantum wells. Here, using double quantum coherence spectroscopy (DQCS), we directly resolve spatial and energetic correlation between excitons in mixed quasi-2D perovskites.

Quasi-2D methylammonium lead iodide $MA_{n-1}Pb_nI_{3n+1}$ perovskites consist of domains of varying number of lead layers, n, separated by a bulky organic cation, such as phenylethylammonium, which acts as a barrier between layered domains (Figure 1a). Strong dielectric[7] and quantum confinement caused by this barrier results in increased exciton binding energies,[4,8] blue shifts the band edge,[4,9] and increases the stability[2,10,11] of quasi-2D perovskites over their bulk counterparts. In other highly excitonic materials such as semiconductor nanostructures, ultrafast four-wave mixing spectroscopies, such as transient absorption, DQCS, and two-dimensional electronic spectroscopy, have been the standard for investigating coherent dynamics of excitons,[12−14] including exciton localization[15,16] and exciton−exciton scattering[13] because of their capacity to probe sensitively the nonlinear response of excitons.[12,14] However, when applied to quasi-2D perovskite systems, previous experiments have lacked sufficient time resolution to observe exciton scattering;[17,18] yet such observations could yield fundamental insight into interwell coupling mechanisms and exciton localization.

DQCS, a variant of transient four-wave mixing spectroscopy, reports on the third-order, nonlinear optical response of a material subsequent to three light−matter interactions[19,20] (Figure 1b and Experimental Methods). In the time domain, DQCS probes the relative time scale over which correlations between excitons in the material decay via the loss of coherent oscillations with time. Initially, the laser field generates a coherence (a superposition of the ground and photoexcited states) in the material with a spatial extent corresponding to the size of the induced polarization. Because the "pump" is two degenerate interactions, the manifold of doubly excited states is accessed, yielding superpositions of the ground and doubly excited states, i.e. double quantum coherences. We observe these coherences as oscillations in time, t_2, with a defined frequency and phase relative to the incident field. This phase

Received: June 24, 2017
Accepted: August 2, 2017
Published: August 2, 2017

DOI: 10.1021/acs.jpclett.7b01621
J. Phys. Chem. Lett. 2017, 8, 3895−3901

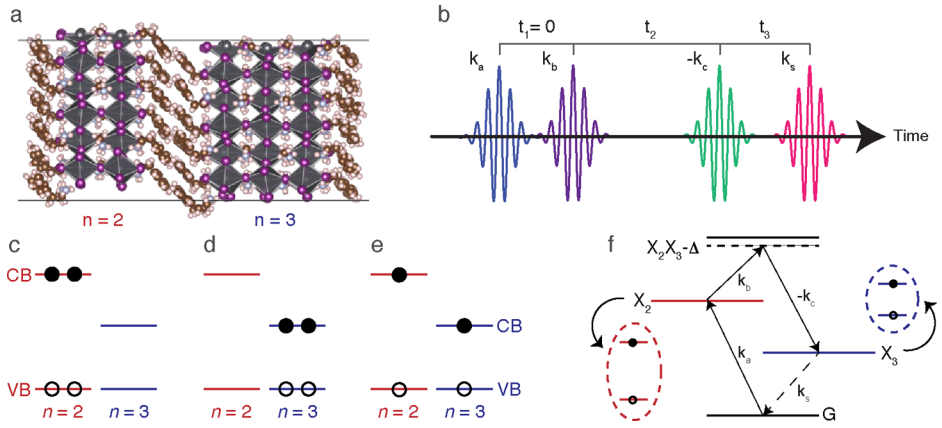

Figure 1. Two-exciton states in quasi-2D perovskites. (a) Quasi-2D perovskite unit cell after ab initio molecular dynamics run and geometry relaxation for $n = 2$ and $n = 3$ domains. (b) Pulse sequence for the DQCS experiments showing wave forms for the three laser pulses and the emitted signal, k_s. (c, d) Electron/hole configurations for a biexciton within each domain and the interwell two-exciton state (e) in the electron/hole basis. (f) Energy diagram showing an example path to an interwell two-exciton state with correlation energy Δ in the exciton basis.

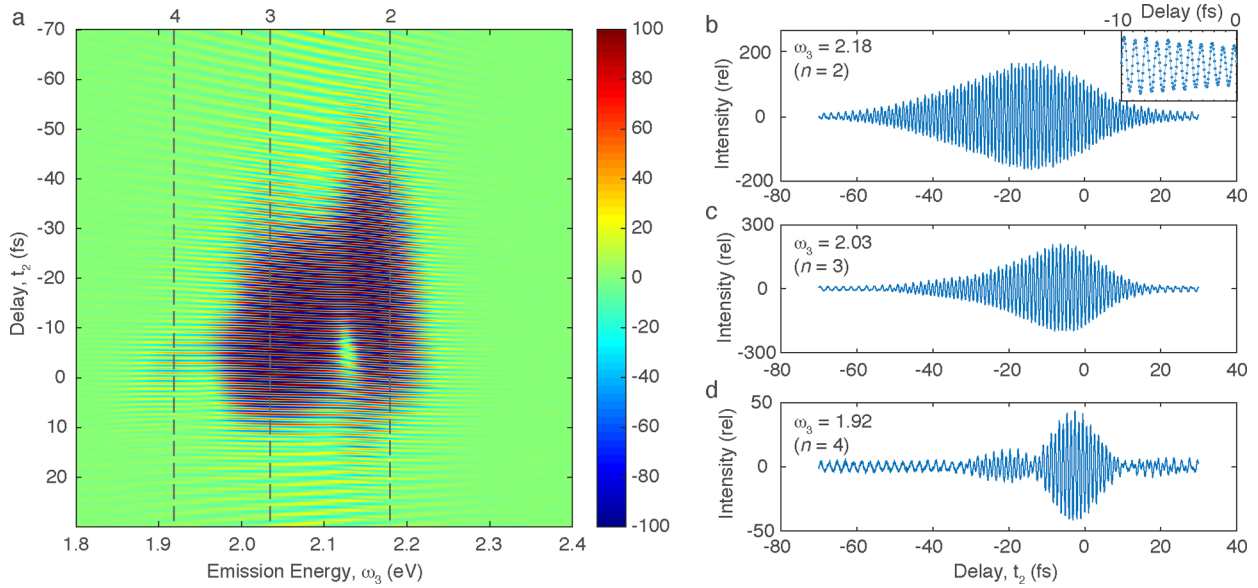

Figure 2. Time domain double quantum data. (a) Time domain double quantum coherence spectrum. Dotted lines indicate the maximum in the linear absorption spectrum associated with the exciton each domain. (b–d) Integrated intensity at the $n = 2$–4 emission energies as a function of t_2. (b inset) Double quantum data from −10 to 0 fs at $n = 2$, showing the ∼1 fs period of the double quantum oscillations.

relationship is subsequently destroyed by scattering processes within the material, including exciton–phonon, exciton–exciton, and exciton–carrier interactions. Because the scattering probability decreases and coherent oscillations dephase more slowly as the exciton becomes more localized,[15,21] the dephasing time of the coherence yields information on the degree of localization in a particular perovskite domain.

In the frequency domain, DQCS reveals correlations between the doubly and singly excited states. The double excitation axis in the frequency domain spectrum is formed by Fourier transformation of the oscillations along t_2 in the time domain. Because the DQCS signal corresponds exclusively to those states for which ground-to-singly and singly-to-doubly excited-state transitions are nondegenerate,[22,23] DQCS in the electronic energy regime is a probe of correlation energy[22] (in the vibrational energy regime, it is sensitive to anharmonicity[24]). Many-body interactions are the mutual Coulomb interaction of more than one exciton or carrier, i.e. correlation;[25−27] therefore, DQCS is a means to investigate selectively features arising from four-body (two-electron, two-hole) states (Figure 1c–e). An example path to an interwell four-body state showing the correlation energy, Δ, is shown in Figure 1f. These four-body states include "unbound-but-correlated" two-exciton states as well as bound biexcitons within a single well (Figure 1c,d) and correlated two-exciton states coupling excitons in neighboring wells (Figure 1e).

Here we investigate the origin of excitonic delocalization in quasi-2D perovskites, both via exciton scattering within a domain and via the interwell excitonic coupling, using DQCS. In the time domain, we observe rapidly decreasing dephasing times for larger n domains (but still $n < 4$), indicating that exciton–exciton scattering rates and exciton delocalization increase with increasing n. Inhomogeneity in the exciton transition frequency, as a result of disorder, contributes minimally to the DQCS data, indicating that localization of the exciton state is governed by the confining potential imparted by the thickness of the well and not "radially" by structural defects in the perovskite, such as in growth

DOI: 10.1021/acs.jpclett.7b01621
J. Phys. Chem. Lett. 2017, 8, 3895−3901

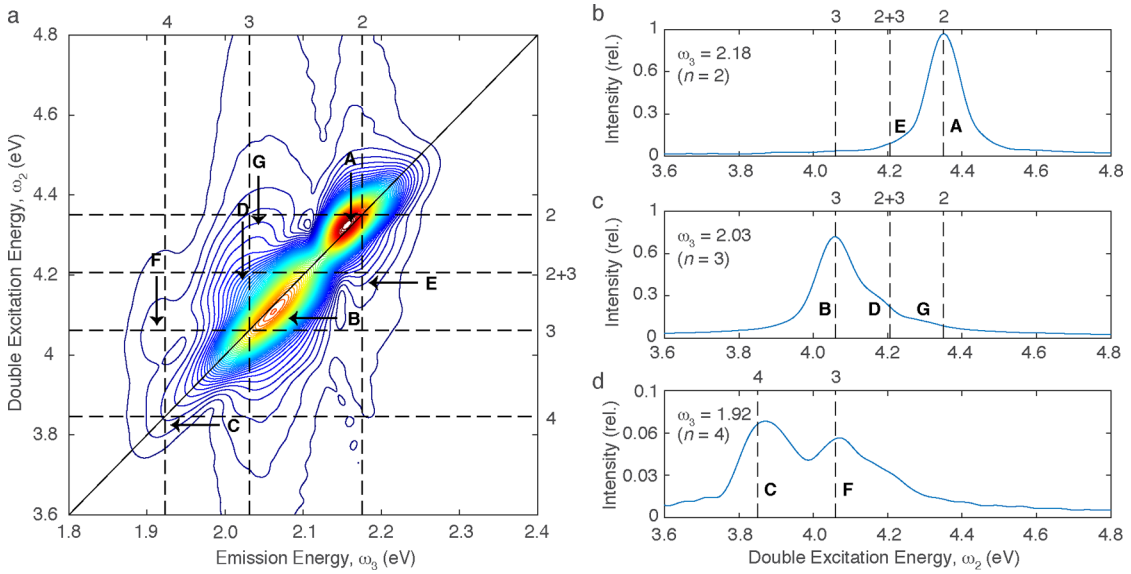

Figure 3. Frequency domain double quantum data. (a) Double quantum coherence spectrum. Dotted vertical lines indicate emission at each maximum in the linear absorption spectrum, and horizontal lines indicate excitation at twice each maximum. (b–d) Slices along the double excitation axis for emission at $n = 2$ to $n = 4$. In panels b and c, vertical lines are shown at double the absorption maxima for $n = 2$, $n = 3$, and the sum of $n = 2$ and $n = 3$. In panel d, vertical lines are shown at double the $n = 2$–4 maxima.

interrupted quantum wells. In the spectral domain, we observe evidence for bound biexcitons in $n = 2$. Additionally, we conclusively identify a delocalized, interwell two-exciton state between the $n = 2$ and $n = 3$ domains (Figure 1e). This state couples the excitons in $n = 2$ and $n = 3$, the most confined domains, and modifies the transfer rate between these wells in applications with high exciton density such as light-emitting diodes.

The time domain data are shown in Figure 2, plotted with time delays positive to negative from bottom to top. The frequency of the oscillations in Figure 2 relates to the energy of the two-quantum coherence excited by the pulse pair, and the signal envelope as a function of time maps the decay of the phase relationship between the driving field of the pulse pair and the induced polarization in the material due to scattering processes. As shown in Figure 2a, there are prominent features in the data near the maxima in the linear absorption spectrum associated with each exciton transition, indicated by dotted lines. Most prominent are two large features at 2.18 eV, $n = 2$ and 2.03 eV, $n = 3$, and a smaller feature at 1.92 eV, $n = 4$. In each individual domain, the maximum amplitude of the oscillation occurs at negative time, −13 fs in $n = 2$, −6 fs in $n = 3$, and −3 fs in $n = 4$.

As shown in Figure 2a, the central emission energy of the oscillating signal associated with each individual domain shifts to lower energy for increasing negative delay, see for example $n = 2$ in Figure 2a. Because all transitions within the laser bandwidth are excited, the shift is an indication of frequency-dependent dephasing. For $n = 3$, the center of the exciton resonance in the linear absorption spectrum (marked with a dotted line) has the longest dephasing time and the latest delayed rise; however, for $n = 2$ the latest delayed rise is well below the exciton resonance. Within a single domain, frequencies higher than the exciton transition in $n = 2$ and 3 have the shortest dephasing times and the earliest onset rise.

In addition to revealing differences in dephasing times within a domain, differences in dephasing times between domains are evident in the double quantum data by taking slices through the intensity as a function of time at the $n = 2$, 3, and 4 exciton resonances, as shown in Figure 2b–d. The inset in Figure 2b shows data from −10 to 0 fs for $n = 2$, plotted as points, with 50 attosecond steps (see Experimental Methods). We observe clear oscillations every ∼1 fs (4 eV), roughly twice the excitation energy. The traces are fit by a Gaussian convoluted cosine function with exponential rise and decay terms. We find best fits to the envelope when the rise and fall times are equivalent, 22.4 ± 0.3 fs, 9.1 ± 0.3 fs, and <5 fs for $n = 2$, 3, and 4, respectively. For $n < 4$, the rise and fall times for the oscillating components increase as the number of Pb_nI_{3n+1} layers decreases.

Finally, we stress that the time domain double quantum measurements are a map of the induced field generated in the material by the laser and not the evolution of an excited-state population. In fact, direct excitation of an excited population is not possible because of the "negative" time ordering of the pulses, relative to a transient grating experiment, which is required to specify the phase-matching condition. The field dependence of the measurement is evidenced by the presence of oscillations in the time domain data with a shorter period than the pulse duration (Figure 2b, inset). Therefore, our time resolution for the oscillating components is dictated by the relative phase stability of the three beams (better than 10 attoseconds[28]) and not the Gaussian width of the pulse envelope (∼10.5 fs). By contrast, the damping terms associated with the oscillation, dictated by the envelope function of the oscillations with time, are limited by the width of the pulse envelope.

Frequency domain double quantum coherence spectra are obtained by Fourier transformation along the delay axis, t_2, yielding the new axis, ω_2, the double quantum excitation energy. In Figure 3a, the double quantum spectrum is shown. The position of a feature in the vertical axis ω_2 is the energy of the double quantum coherence excited by the pulse pair, and in the horizontal axis ω_3, the single-quantum emission (detection) energy. The diagonal line indicates the case where the emission energy is exactly twice the excitation energy, $\omega_2 = 2\omega_3$. Dotted

DOI: 10.1021/acs.jpclett.7b01621
J. Phys. Chem. Lett. 2017, 8, 3895–3901

lines are drawn at double the energy of the exciton resonances in each domain in ω_2 and at the exciton resonances in ω_3. Because t_1 is fixed at zero and the t_2 axis was Fourier transformed into the frequency domain, there is no time axis for this measurement.

On the diagonal, there are prominent features at the exciton resonances for $n = 2$, feature A, and $n = 3$, feature B. Feature A is shifted along the diagonal to lower energy, while feature B is extended on the diagonal both to lower and higher energy. At $n = 4$, feature C is of low amplitude but largely on the resonance. Off the diagonal, we observe intensity above the diagonal, feature D, which is mirrored more weakly below the diagonal by feature E. Features D and E correspond to excitation at the sum of $n = 2$ and $n = 3$ and emission at $n = 3$ and 2, respectively. Finally, a second feature above the diagonal, feature F, connects double excitation at $n = 3$ to emission at $n = 4$.

Spectral slices (Figure 3b–d) taken at each exciton emission energy allow for evaluation of the double quantum data in greater detail. As a guide, vertical lines are positioned at twice the energy of each individual exciton resonance and at the sum of the energies of $n = 2$ and $n = 3$. Figure 3b shows primarily feature A at $n = 2$ with a skew of the Lorentzian to lower energy due to feature E. The spectrum in Figure 3c is fit with three Lorentzians first at $n = 3$, feature B; second below the sum of $n = 2$ and 3, feature D; and third at a higher energy feature, feature G. Finally, the spectrum in Figure 3d shows prominent features at $n = 3$, feature C; $n = 4$, feature F; and a broad higher-energy feature. The slices of the frequency domain data at each emission frequency clearly show cross-peaks D, E, F, and G and their respective positions on the double excitation axis.

In Figure 4, the trace of the double quantum spectrum taken along the diagonal is shown plotted as a function of the double

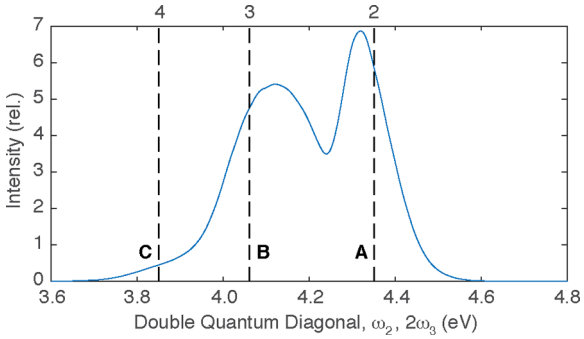

Figure 4. Double quantum diagonal. The diagonal of the double quantum coherence spectrum plotted on the double quantum axis. Vertical lines are shown at double the absorption maxima for $n = 2$–4.

quantum axis. The spectrum shows three features near each of the exciton resonances, features A, B, and C in Figure 3. Feature A is peaked below the $n = 2$ exciton transition. By fitting the spectrum in Figure 4 to three Lorentzians, we find feature A is shifted 15 meV to lower energy. Though feature B peaks above the $n = 3$ exciton resonance, feature B is largely broadened with less spectral intensity below the resonance than feature A.

In the time domain, four-wave mixing data are a map of the evolving field generated in the material; therefore, the signal can be observed as long as a phase relationship exists between the driving field and the responding field. As seen in Figure 2, a delayed rise in the time domain signal is observed for all perovskite domain sizes in the negative delay direction. Rephasing of the polarization coherence masked by inhomogeneity in the transition frequency is the prototypical cause of such delayed rises in four-wave mixing experiments, which are called photon-echoes by analogy to spin-echoes in nuclear magnetic resonance. In a photon-echo, inhomogeneity in the response results in loss of observable polarization coherence, though individual transitions may yet retain a fixed phase relative to the driving field. In order to form a photon-echo, polarization coherence is "rephased" by a subsequent interaction creating a recurrence in the signal.

In addition to traditional spectral inhomogeneity, semiconductors may exhibit an additional contribution to the polarization coherence decay time due to many-body scattering. GaAs quantum wells are a classical example of this effect. These quantum wells can be prepared with atomically precise well thickness, so inhomogeneity in the transition frequency due to variations in the confining potential can be effectively minimized. In a series of seminal experiments, homogeneously broadened samples were shown to exhibit pronounced delayed rise times despite a lack of spectral inhomogeneity,[29−31] which could be assigned only to variations in the transition frequency caused by scattering with another exciton.[14] This additional contribution to the inhomogeneous line width caused by many-body scattering is called excitation-induced dephasing, while the renormalization of the transition frequency due to many-body interaction is called excitation-induced shift.[12] In a double quantum experiment, both effects allow for loss of observable polarization coherence and an echo in a similar manner to an inhomogeneous environment.

However, inhomogeneous dephasing and excitation-induced effects should have different trends in the lifetime of the coherence as a function of confinement. In the limit of dominant many-body scattering, decreasing confinement increases the Bohr radius, and the excited species becomes more delocalized. As the exciton delocalizes, the scattering probability increases and the dephasing time becomes shorter. However, in the inhomogeneous case, inhomogeneity becomes increasingly likely as the well becomes thicker because of well width variations, point defects, etc. that will tend to localize the exciton wave function and thus lengthen the recurrence time. Increasing inhomogeneous broadening thus results in the opposite trend from many-body scattering: longer dephasing times for decreasing confinement. Therefore, to determine the relative importance of each route to localization in perovskite wells, we can compare the dephasing time for varying degree of confinement, n.

The dephasing time associated with the rise and fall time of the oscillations gets shorter with decreasing confinement, by domain 22.4 ± 0.3 fs, 9.1 ± 0.3 fs, and <5 fs for $n = 2$, 3, and 4, respectively; therefore, this suggests that the dominant factor in the polarization coherence decay is the many-body scattering rate, which slows as excitons localize in more confined domains. The same argument can be extended to explain the variation of the dephasing times within a domain. Within a single domain, the correlation energy is highest near the band edge at transitions with the strongest biexciton binding energy (redder absorbing). The longer dephasing times for the reddest emitting two-exciton coherences arise from the net binding exciton−exciton interaction near the band edge, which increases the correlation time within a domain and results in the apparent red shift of each individual domain in the time domain data in Figure 2a.

DOI: 10.1021/acs.jpclett.7b01621
J. Phys. Chem. Lett. 2017, 8, 3895−3901

In related two-dimensional electronic spectroscopy measurements, excitation-induced dephasing results in excitation frequency-dependent broadening in the rephasing spectra.[32] This has been used to distinguish excitation-induced dephasing from spectral inhomogeneity in GaAs.[12,32,33] In the Supporting Information, we show the rephasing and nonrephasing two-dimensional electronic spectra. We observe strong line broadening of the single exciton transitions in the rephasing spectra of striking similarity to GaAs. These line shapes are in strong support of the dominant role of excitation-induced dephasing in polarization coherence decay times in quasi-2D perovskite.

Our time domain results in quasi-2D perovskites show marked differences from their bulk counterparts in that many-body effects are clearly evident. The driving force for delocalization in bulk perovskites has been discussed recently based on comparative analysis of transient four-wave mixing spectra of cold perovskite and GaAs.[6] These data show that dephasing in bulk perovskite is three times slower than bulk GaAs because of *weak* many-body interaction (carrier−carrier scattering). Additionally, based on analysis of optical Kerr effect spectroscopy of bulk perovskite, it has been suggested that weak many-body scattering in the bulk is due to increased screening of charge carriers by reorientation of the methylammonium cation and/or shallow local potential defects in the perovskite lattice.[34] In contrast with bulk perovskite where many-body interactions may be effectively screened, we demonstrate that many-body scattering dominates the nonlinear response of the most confined perovskite wells.

In the frequency domain, the DQCS spectrum is a frequency−frequency map correlating doubly excited, two-exciton states with single exciton states. Features on the diagonal correspond to interaction between excitons at the same frequency, such as features A, B, and C in Figure 3a. As shown from prior experimental[26] and theoretical work,[35] biexcitons within a single domain (Figure 1c,d) appear in DQCS data as features excited at twice the single exciton transition energy less the biexciton binding energy and emitting at the single exciton transition energy less the binding energy $(\omega_I - \Delta, 2\omega_I - \Delta)$. This results in a feature on the diagonal shifted below the exciton resonance by Δ.

The three features observed on the diagonal in Figure 3a have increasing contributions from bound two-exciton states with increasing confinement, evidenced by the increasing intensity below the exciton resonance in Figure 4. A single Lorentzian fit to feature A yields a shift of 15 meV below the exciton resonance; however, because of limitations in both the spectral bandwidth and the width of feature A, 15 meV is an upper bound on the n = 2 biexciton binding energy, much smaller than the exciton binding energy in n = 2 of 260 meV.[4] The reported biexciton binding energy agrees reasonably with prior reports of the biexcition binding energy of cold n = 1 perovskite of ∼40 meV.[36] Also on the diagonal, we observe strong elongation above and weaker elongation below the diagonal of feature B, associated with n = 3, as shown in Figure 4. These results suggest an even smaller, if not negligible, biexciton binding energy in n = 3. Increasing biexciton binding energies for increasing confinement, as shown here, is typical in other highly confined systems, including single-domain perovskite quantum wells,[36,37] semiconducting quantum dots,[38] and transition-metal dichacolgenides.[39]

Off-diagonal features, cross-peaks, correspond to interaction between excitons at differing frequencies, such as features D, E, F, and G in Figure 3. A cross-peak at the double excitation energy of one domain and at the emission energy of another $(\omega_I, 2\omega_{II})$, such as features F and G, indicates coupling between single exciton states in different domains.[35] These second harmonic oscillations corresponding to a neighboring exciton resonance occur when excitons in neighboring wells are electronically coupled, for example, by hybridization of the electron, hole, or exciton states between wells. Though typically characterized by the longer $\omega_I - \omega_{II}$ oscillations,[40] coupling between single excitons neighboring wells is observable even when the dephasing time is much shorter than the $\omega_I - \omega_{II}$ period, due to the higher frequency of the second harmonic oscillations. An example path to a feature at $(\omega_I, 2\omega_{II})$ and its relationship to coupling in the singly excited manifold is shown in the Supporting Information.[41] In order to form features F and G, a doubly excited state is not required to couple the two wells because electronic coupling already exists in the single exciton manifold.

Conversely, a cross-peak at the sum of excitation energies of two different domains and emitting at the single exciton energies $(\omega_I, \omega_I + \omega_{II})$ can occur only if an exciton in each well is excited in sequence (Figure 1f). A cross-peak at this position implies that a doubly excited state coupling both domains exists (Figure 1e). Conceptually, this means that two excitons in differently confined wells scatter, resulting in an additional contribution to the four-body Coulomb interaction. Features D and E are indicative of this second case and are identified as an interwell, two-exciton state connecting n = 2 and n = 3.[41] We observe little shift of features D and E from the sum of the n = 2 and n = 3 exciton energies, so we conclude that this is a more weakly bound two-exciton interaction than observed within a single domain.

Features D and E are best assigned to a two-exciton state coupling n = 2 and n = 3 domains through the phenylethylammonium layer (Figure 1e). Coupling between domains of varying width not separated by a barrier, for instance due to a well width fluctuation, would result in a strong inhomogeneous contribution to the polarization coherence dephasing time, which we do not observe. In order to test the effect of increased spatial inhomogeneity, we compare DQCS data from hot-cast films versus films cast at room temperature, which should show significantly decreased spatial irregularity based on GIWAXS data.[3,42] DQCS data from hot cast films do not show a significant difference from room-temperature films beyond an increase in n = 2 in the hot cast films.[41] Additionally, DQCS data on films synthesized from n = 2 nanoplatelets with substantially less n = 3+ show reduced cross-peaks and longer dephasing times in n = 2, consistent with reduction in interwell scattering states.[41] Finally, a precedent for such interactions exists in GaAs quantum wells. Two-exciton interwell states were identified in GaAs/InGaAs quantum wells and were attributed to a 0.15 meV shift of the exciton resonance due to many-body scattering.[27]

Stronger features at the interwell two-exciton state and minimal crosspeaks at twice the single exciton energies in the DQCS data demonstrate that coupling between the n = 2 and n = 3 domains does not arise solely from hybridization of the electron/hole wave functions or dipole−dipole coupling; instead, two-exciton states result from exciton−exciton scattering between domains. Additionally, though the interwell doubly excited states contribute the largest cross-peaks between n = 2 and n = 3, the cross-peaks between n = 3 and 4 are primarily between single exciton states. On the basis of the

DOI: 10.1021/acs.jpclett.7b01621
J. Phys. Chem. Lett. 2017, 8, 3895−3901

emergence of these cross-peaks for higher n domains, we expect that electronic coupling between single exciton states should increase for larger n domains.

In summary, we have used DQCS to investigate the various routes to excitonic delocalization in quasi-2D perovskite. We have demonstrated that the coherent response in confined perovskite is dominated by many-body scattering. Within an individual domain, we have shown that localization is driven by the confining potential imparted by the phenylethylammonium layer, which increases the exciton binding energy. This is evidenced by the decreasing dephasing time of the two-exciton coherences in the time domain data as the number of perovskite layers increases, which we attributed to decreased exciton−exciton scattering. In conjunction with optical Kerr effect data,[34] we postulate that the driving force for localization differs in confined perovskite, where excitations are localized as excitons, from bulk perovskite, where excitation is localized as free carriers. Additionally, we have shown that the spatial extent of the exciton state within a well is resistant to the localizing effect of inhomogeneity, allowing excitons to better navigate disorder.

Furthermore, we have demonstrated both the presence of bound biexcitons within a single perovskite domain and an interwell two-exciton state. This interwell state provides a source of excitonic coupling beyond that provided in the singles manifold alone, such as dipole−dipole coupling or hybridization of the electron/hole states between domains. The interwell state contributes the dominant features in the DQCS data for the most confined domains. As a parallel to effects in quantum cascade lasers[43] where many-body correlations were shown to affect the tunneling rate between quantum wells,[44,45] these results suggest that population transfer between domains under high photon flux and in the most confined perovskite domains can be affected by many-body correlations.

EXPERIMENTAL METHODS

Materials studied here are 200 nm thick films of median n equal to 3 with contributions from n = 2−4, similar to those described previously,[2] and prepared by the procedure in the supplement.[41] In a DQCS experiment, the nonlinear optical response of a material is measured subsequent to excitation using the pulse sequence shown in Figure 1b. The delay, t_1, between pulse pair, k_a and k_b, is fixed at zero, and the delay between k_c and the pulse pair, t_2, is varied by moving k_a and k_b together in time. Due to the geometry of the interacting pulses, the radiated signal, k_s, is the difference between the pulse pair, $k_a + k_b$, and the "probe", k_c, obeying the phase matching condition, $k_s = k_a + k_b - k_c$. DQCS data are acquired using a two-dimensional electronic spectroscopy setup described previously[28,46] in the BOXCARS geometry and using a procedure also previously described.[19,22] All three pulses have an identical spectrum centered at 2.1 eV, spanning 1.8−2.3 eV, and compressed to a duration of ∼10.5 fs.[41] Additionally, all beams have parallel polarization; therefore, bound four-body states and unbound four-body scattering states are both detected.[35,47]

ASSOCIATED CONTENT

Supporting Information

The Supporting Information is available free of charge on the ACS Publications website at DOI: 10.1021/acs.jpclett.7b01621.

Absorption spectrum, extended methods, transient-grating frequency-resolved optical gating trace, rephasing two-dimensional electronic spectrum, DQCS data on hot-cast and room-temperature cast films, DQCS data on n = 2 films, additional notes on the analysis of frequency domain DQCS data (PDF)

AUTHOR INFORMATION

Corresponding Author

*E-mail: gscholes@princeton.edu.

ORCID

Madeline H. Elkins: 0000-0001-5076-8577
Oleksandr Voznyy: 0000-0002-8656-5074
Shana O. Kelley: 0000-0003-3360-5359
Gregory D. Scholes: 0000-0003-3336-7960

Author Contributions

M.H.E. wrote the manuscript with substantive contribution from and discussion with all authors. M.H.E. preformed the DQCS experiments and analyzed the data. R.P. and A.H.P. assisted in analysis of the DQCS data. Theoretical calculations were performed by O.V. A.H.P and L.N.Q. synthesized the Q2D perovskite thin films. Correspondence and requests for materials should be addressed to G.D.S. (gscholes@princeton.edu) or E.H.S. (ted.sargent@utoronto.ca).

Notes

The authors declare no competing financial interest.

ACKNOWLEDGMENTS

M.H.E., E.H.S., and G.D.S. gratefully acknowledge the support of the Canadian Institute for Advanced Research through its Bio-Inspired Solar Energy program. A.H.P. is supported by the Fonds de Recherche du Québec- Nature et Technologies. Additionally, E.H.S. acknowledges the Ontario Fund: Research Excellence Program, the Natural Sciences and Engineering Research Council of Canada, and a University of Toronto Connaught grant. G.D.S. thanks Princeton University through the Innovation Fund for New Ideas in the Natural Sciences. M.H.E. thanks the members of the Scholes Group and Karl Leo, Technische Universität Dresden, for helpful discussion regarding the manuscript.

REFERENCES

(1) Chen, S.; Shi, G. Two-dimensional materials for halide perovskite-based optoelectronic devices. *Adv. Mater.* **2017**, *29*, 1605448.

(2) Yuan, M.; Quan, L. N.; Comin, R.; Walters, G.; Sabatini, R.; Voznyy, O.; Hoogland, S.; Zhao, Y.; Beauregard, E. M.; Kanjanaboos, P.; et al. Perovskite energy funnels for efficient light-emitting diodes. *Nat. Nanotechnol.* **2016**, *11*, 872.

(3) Tsai, H.; Nie, W.; Blancon, J. C.; Stoumpos, C. C.; Asadpour, R.; Harutyunyan, B.; Neukirch, A. J.; Verduzco, R.; Crochet, J. J.; Tretiak, S.; et al. High-efficiency two-dimensional Ruddlesden-Popper perovskite solar cells. *Nature* **2016**, *536*, 312.

(4) Tanaka, K.; Kondo, T. Bandgap and exciton binding energies in lead-iodide-based natural quantum-well crystals. *Sci. Technol. Adv. Mater.* **2003**, *4*, 599−604.

(5) Wu, X.; Trinh, M. T.; Zhu, X. Y. Excitonic many-body interactions in two-dimensional lead iodide perovskite quantum wells. *J. Phys. Chem. C* **2015**, *119*, 14714−14721.

(6) March, S. A.; Riley, D. B.; Clegg, C.; Webber, D.; Liu, X.; Dobrowolska, M.; Furdyna, J. K.; Hill, I. G.; Hall, K. C. Four-wave mixing reveals weaker many-body interactions and slower dephasing in

DOI: 10.1021/acs.jpclett.7b01621
J. Phys. Chem. Lett. 2017, 8, 3895−3901

perovskite photovoltaic materials than GaAs. 2016, arXiv preprint arXiv:1602.05186.
(7) Keldysh, L. V. Coulomb interaction in thin semiconductor and semimetal films. *JETP Lett.* **1979**, *29*, 658−661.
(8) Hong, X.; Ishihara, T.; Nurmikko, A. V. Dielectric confinement effect on excitons in PbI_4-based layered semiconductors. *Phys. Rev. B: Condens. Matter Mater. Phys.* **1992**, *45*, 6961−6964.
(9) Ishihara, T.; Takahashi, J.; Goto, T. Optical properties due to electronic transitions in two-dimensional semiconductors $(C_nH_{2n+1}NH_3)_2PbI_4$. *Phys. Rev. B: Condens. Matter Mater. Phys.* **1990**, *42*, 11099.
(10) Smith, I. C.; Hoke, E. T.; Solis-Ibarra, D.; McGehee, M. D.; Karunadasa, H. I. A layered hybrid perovskite solar-cell absorber with enhanced moisture stability. *Angew. Chem.* **2014**, *126*, 11414.
(11) Quan, L. N.; Yuan, M.; Comin, R.; Voznyy, O.; Beauregard, E. M.; Hoogland, S.; Buin, A.; Kirmani, A. R.; Zhao, K.; Amassian, A.; et al. Ligand-stabilized reduced-dimensionality perovskites. *J. Am. Chem. Soc.* **2016**, *138*, 2649−2655.
(12) Cundiff, S. T. Coherent spectroscopy of semiconductors. *Opt. Express* **2008**, *16*, 4639−4664.
(13) Chemla, D. S.; Shah, J. Many-body and correlation effects in semiconductors. *Nature* **2001**, *411*, 549−557.
(14) Shah, J. *Ultrafast Spectroscopy of Semiconductors and Semiconductor Nanostructures*; Springer Science: Berlin, 2013; Vol. *115*.
(15) Hellmann, R.; Cundiff, S. T.; Koch, M.; Feldmann, J.; Gobel, E. O.; Kuhn-Heinrich, B.; Yakovlev, D. R.; Waag, A.; Landwehr, G. Exciton dynamics in disordered quantum wells: Localized and delocalized regimes. *Phys. Rev. B: Condens. Matter Mater. Phys.* **1994**, *50*, 14651−14654.
(16) Hegarty, J.; Sturge, M. D. Studies of exciton localization in quantum-well structures by nonlinear-optical techniques. *J. Opt. Soc. Am. B* **1985**, *2*, 1143−1154.
(17) Wu, X.; Trinh, M. T.; Niesner, D.; Zhu, H.; Norman, Z.; Owen, J. S.; Yaffe, O.; Kudisch, B. J.; Zhu, X. Y. Trap states in lead iodide perovskites. *J. Am. Chem. Soc.* **2015**, *137*, 2089.
(18) Hassan, Y.; Song, Y.; Pensack, R. D.; Abdelrahman, A. I.; Kobayashi, Y.; Winnik, M. A.; Scholes, G. D. Structure-tuned lead halide perovskite nanocrystals. *Adv. Mater.* **2016**, *28*, 566−573.
(19) Kim, J.; Mukamel, S.; Scholes, G. D. Two-dimensional electronic double-quantum coherence spectroscopy. *Acc. Chem. Res.* **2009**, *42*, 1375.
(20) Cundiff, S. T.; Zhang, T.; Bristow, A. D.; Karaiskaj, D.; Dai, X. Optical two-dimensional fourier transform spectroscopy of semiconductor quantum wells. *Acc. Chem. Res.* **2009**, *42*, 1423−1432.
(21) Lonsky, C.; Thomas, P.; Weller, A. Optical dephasing in disordered semiconductors. *Phys. Rev. Lett.* **1989**, *63*, 652−655.
(22) Kim, J.; Huxter, V. M.; Curutchet, C.; Scholes, G. D. Measurement of electron-electron interactions and correlations using two-dimensional electronic double-quantum coherence spectroscopy. *J. Phys. Chem. A* **2009**, *113*, 12122−12133.
(23) Mukamel, S.; Oszwaldowski, R.; Yang, L. A coherent nonlinear optical signal induced by electron correlations. *J. Chem. Phys.* **2007**, *127*, 221105.
(24) Fulmer, E. C.; Mukherjee, P.; Krummel, A. T.; Zanni, M. T. A pulse sequence for directly measuring the anharmonicities of coupled vibrations: Two-quantum two-dimensional infrared spectroscopy. *J. Chem. Phys.* **2004**, *120*, 8067−8067.
(25) Stone, K. W.; Gundogdu, K.; Turner, D. B.; Li, X.; Cundiff, S. T.; Nelson, K. A. Two-quantum 2D FT electronic spectroscopy of biexcitons in GaAs quantum wells. *Science* **2009**, *324*, 1169.
(26) Karaiskaj, D.; Bristow, A. D.; Yang, L.; Dai, X.; Mirin, R. P.; Mukamel, S.; Cundiff, S. T. Two-quantum many-body coherences in two-dimensional fourier-transform spectra of exciton resonances in semiconductor quantum wells. *Phys. Rev. Lett.* **2010**, *104*, 117401.
(27) Nardin, G.; Moody, G.; Singh, R.; Autry, T. M.; Li, H.; Morier-Genoud, F.; Cundiff, S. T. Coherent excitonic coupling in an asymmetric double InGaAs quantum well arises from many-body effects. *Phys. Rev. Lett.* **2014**, *112*, 046402.
(28) Turner, D. B.; Wilk, K. E.; Curmi, P. M. G.; Scholes, G. D. Comparison of electronic and vibrational coherence measured by two-dimensional electronic spectroscopy. *J. Phys. Chem. Lett.* **2011**, *2*, 1904.
(29) Kim, D. S.; Shah, J.; Damen, T. C.; Schafer, W.; Jahnke, F.; Schmitt-Rink, S.; Kohler, K. Unusually slow temporal evolution of femtosecond four-wave-mixing signals in intrinsic GaAs quantum wells: Direct evidence for the dominance of interaction effects. *Phys. Rev. Lett.* **1992**, *69*, 2725−2728.
(30) Leo, K.; Wegener, M.; Shah, J.; Chemla, D. S.; Gobel, E. O.; Damen, T. C.; Schmitt-Rink, S.; Schafer, W. Effects of coherent polarization interactions on time-resolved degenerate four-wave mixing. *Phys. Rev. Lett.* **1990**, *65*, 1340−1343.
(31) Wang, H.; Ferrio, K.; Steel, D. G.; Hu, Y. Z.; Binder, R.; Koch, S. W. Transient nonlinear optical response from excitation induced dephasing in GaAs. *Phys. Rev. Lett.* **1993**, *71*, 1261.
(32) Li, X. Q.; Zhang, T. H.; Mukamel, S.; Mirin, R. P.; Cundiff, S. T. Investigation of electronic coupling in semiconductor double quantum wells using coherent optical two-dimensional Fourier transform spectroscopy. *Solid State Commun.* **2009**, *149*, 361−366.
(33) Borca, C. N.; Zhang, T.; Li, X.; Cundiff, S. T. Optical two-dimensional Fourier transform spectroscopy of semiconductors. *Chem. Phys. Lett.* **2005**, *416*, 311.
(34) Zhu, H.; Miyata, K.; Fu, Y.; Wang, J.; Joshi, P. P.; Niesner, D.; Williams, K. W.; Jin, S.; Zhu, X. Y. Screening in crystalline liquids protects energetic carriers in hybrid perovskites. *Science* **2016**, *353*, 1409.
(35) Yang, L.; Mukamel, S. Dissecting quantum pathways in two-dimensional correlation spectroscopy of semiconductors. *J. Phys.: Condens. Matter* **2008**, *20*, 395202.
(36) Ishihara, T.; Hong, X.; Ding, J.; Nurmikko, A. V. Dielectric confinement effect for exciton and biexciton states in PbI4-based two-dimensional semiconductor structures. *Surf. Sci.* **1992**, *267*, 323−326.
(37) Kondo, T.; Azuma, T.; Yuasa, T.; Ito, R. Biexciton lasing in the layered perovskite-type material $(C_6H_{13}NH_3)_2PbI_4$. *Solid State Commun.* **1998**, *105*, 253−255.
(38) Moody, G.; Singh, R.; Li, H.; Akimov, I. A.; Bayer, M.; Reuter, D.; Wieck, A. D.; Bracker, A. S.; Gammon, D.; Cundiff, S. T. Influence of confinement on biexciton binding in semiconductor quantum dot ensembles measured with two-dimensional spectroscopy. *Phys. Rev. B: Condens. Matter Mater. Phys.* **2013**, *87*, 041304.
(39) You, Y.; Zhang, X.-X.; Berkelbach, T. C.; Hybertsen, M. S.; Reichman, D. R.; Heinz, T. F. Observation of biexcitons in monolayer WSe_2. *Nat. Phys.* **2015**, *11*, 477.
(40) Leo, K.; Shah, J.; Gobel, E. O.; Damen, T. C.; Schmitt-Rink, S.; Schafer, W.; Kohler, K. Coherent oscillations of a wave packet in a semiconductor double-quantum-well structure. *Phys. Rev. Lett.* **1991**, *66*, 201−204.
(41) See the Supporting Information.
(42) Milot, R. L.; Sutton, R. J.; Eperon, G. E.; Haghighirad, A. A.; Martinez Hardigree, J.; Miranda, L.; Snaith, H. J.; Johnston, M. B.; Herz, L. M. Charge-carrier dynamics in 2D hybrid metal−halide perovskites. *Nano Lett.* **2016**, *16*, 7001−7007.
(43) Faist, J.; Capasso, F.; Sivco, D. L.; Sirtori, C.; Hutchinson, A. L.; Cho, A. Y. Quantum cascade laser. *Science* **1994**, *264*, 553−556.
(44) Liu, T.; Lee, K. E.; Wang, Q. J. Microscopic density matrix model for optical gain of terahertz quantum cascade lasers: Many-body, nonparabolicity, and resonant tunneling effects. *Phys. Rev. B: Condens. Matter Mater. Phys.* **2012**, *86*, 235306.
(45) Wang, F.; Guo, X. G.; Cao, J. C. Many-body interaction in resonant tunneling of terahertz quantum cascade lasers. *J. Appl. Phys.* **2010**, *108*, 083714.
(46) Turner, D. B.; Dinshaw, R.; Lee, K. K.; Belsley, M. S.; Wilk, K. E.; Curmi, P. M.; Scholes, G. D. Quantitative investigations of quantum coherence for a light-harvesting protein at conditions simulating photosynthesis. *Phys. Chem. Chem. Phys.* **2012**, *14*, 4857.
(47) Zhang, T.; Kuznetsova, I.; Meier, T.; Li, X.; Mirin, R. P.; Thomas, P.; Cundiff, S. T. Polarization-dependent optical 2D Fourier transform spectroscopy of semiconductors. *Proc. Natl. Acad. Sci. U. S. A.* **2007**, *104*, 14227.

DOI: 10.1021/acs.jpclett.7b01621
J. Phys. Chem. Lett. 2017, 8, 3895−3901